The Relationship Between Macula Retinal Ganglion Cell Density and Visual Function in the Nonhuman Primate

Kwame Antwi-Boasiako,[1] Louvenia Carter-Dawson,[2] Ronald Harwerth,[2] Margaret Gondo,[2] and Nimesh Patel[2]

[1]New England College of Optometry, Boston, Massachusetts, United States
[2]College of Optometry, University of Houston, Houston, Texas, United States

Correspondence: Nimesh Patel, University of Houston, College of Optometry, 4901 Calhoun Road, Houston, TX 77204, USA; npatel@central.uh.edu.

Received: April 18, 2020
Accepted: September 29, 2020
Published: January 5, 2021

Citation: Antwi-Boasiako K, Carter-Dawson L, Harwerth R, Gondo M, Patel N. The relationship between macula retinal ganglion cell density and visual function in the nonhuman primate. *Invest Ophthalmol Vis Sci.* 2021;62(1):5. https://doi.org/10.1167/iovs.62.1.5

Purpose. Loss of ganglion cell inner plexiform layer (GCIPL) and visual sensitivity in the macula region are known to occur at all stages of glaucoma. While both are dependent on the underlying retinal ganglion cells (RGCs), the relationship between structure and function is modest. We hypothesize that the imprecise relationship is due to a lack of direct correspondence between in vivo measures and RGC counts, as well as the relatively large stimulus size used by standard perimetry, which exceeds spatial summation.

Methods. The relationship between optical coherence tomography (OCT)–derived GCIPL thickness and corresponding inner cell density from retinal flat mounts was determined for four nonhuman primates with varying stages of neuropathy. Normative data for 10-2 threshold using Goldman size I to V stimuli were established for 10 animals, 4 of which were then followed longitudinally with OCT and perimetry. The relationship between GCIPL volume, which incorporated stimulus size after removal of residual thickness, and differential light sensitivity was determined for both experimental glaucoma and healthy eyes.

Results. Peak inner retinal cell density was 63,052 ± 9238 cells/mm^2 in the healthy eye. Cell density was related to both GCIPL thickness and eccentricity ($R^2 = 0.74$, $P < .01$). For all 10-2 eccentricities, size III stimuli were greater than the critical area ($P < 0.01$). Based on the structural and histologic relationship, the critical area corresponds to approximately 156 RGCs.

Conclusions. The relationship between cell density and GCIPL thickness is dependent on retinal eccentricity. For 10-2 perimetry, perimetric loss, especially at earlier stages of neuropathy, may best be detected using size II or smaller stimuli.

Keywords: perimetry, spatial summation, retinal ganglion cells, optical coherence tomography, ganglion cell inner plexiform layer

Primary open-angle glaucoma is a progressive optic neuropathy that has characteristic losses of retinal ganglion cells (RGCs) and visual sensitivity. The disease is typically described as initially affecting peripheral visual function with central acuity preserved until later stages of neuropathy. However, there is significant evidence of structural and functional losses in areas of high acuity, even at early stages of disease.[1–10] In fact, it has been shown that macular tests of visual function using 10-2 perimetry, in addition to macula optical coherence tomography (OCT) imaging, can be beneficial for glaucoma management.[11]

The macula region has the highest density of RGCs, and in vivo OCT can be used to reliably quantify the inner retinal thickness. Because the ganglion cell layer becomes difficult to visualize with mild to moderate RGC loss, the inner retina is often quantified as the ganglion cell–inner plexiform layer (GCIPL) and/or ganglion cell complex (GCC), which both have excellent reproducibility.[12–14] Measures of the GCC include RGC axons, some of which may be from distal cell bodies. In contrast, GCIPL includes the cell body and dendrites, which are likely a better representation of localized RGC content. The common macula OCT scan protocols include all of the 68 test locations sampled by the 10-2 perimetry protocol, and ideally there should be good correspondence between in vivo thickness measures and visual sensitivity after accounting for RGC displacement.[15] However, the relationship between visual sensitivity and inner retinal thickness is only modest, with significant losses in structural thickness prior to measurable loss of visual function.[16–18] We hypothesize that this imprecise relationship is due to (1) a lack of direct correspondence of RGC counts to GCIPL thickness and (2) the relatively large stimulus size used by standard perimetry (Goldmann size III), which exceeds the critical area of complete spatial summation.

In the first instance, when assessing OCT-derived inner retinal thickness, there is an assumption of a linear relationship with cell counts. However, there are differences in RGC distribution with retinal eccentricity, and the RGC density is greatest in the macula region, where cells are also smaller in size.[19–22] Thus, one of the objectives of this experiment was to establish the relationship between OCT-derived GCIPL

Copyright 2021 The Authors

This work is licensed under a Creative Commons Attribution-NonCommercial-NoDerivatives 4.0 International License.

Downloaded from iovs.arvojournals.org on 01/18/2023

thickness and histologic measures of RGC density in healthy and glaucomatous eyes.

With respect to spatial summation and visual sensitivity, the standard stimulus size used for quantifying visual function is the Goldmann III (0.43° in diameter), which exceeds spatial summation (Ricco's law) in the central macula region.[23–25] Ricco's law states that visual thresholds decrease with increase in stimulus size, with a slope of −1 (log-log axis), when stimuli are smaller than a critical area (Ac).[26] However, when stimuli are larger than the Ac, and pooling is from a larger number of detector elements, the slope of this function is shallower. Hence, at early stages of neuropathy, a loss of RGCs results in functional losses, which may be less than the normal measurement variability when assessed with Goldmann size III perimetry, which exceeds Ac. In principle, use of stimuli at or smaller than Ac would result in thresholds that are proportional to the RGC number, but these harder-to-see stimuli may also have reduced reliability. Similarly, larger stimuli should have greater reliability but with reduced proportionality and therefore making changes in thresholds less reflective of the underlying RGC counts. However, the relationship between stimulus size and disease progression has not been established.

The nonhuman primate is an ideal experimental model for investigations of structural and functional changes with glaucoma. In fact, the nonlinear model, which was experimentally derived using nonhuman primates, has been successfully translated to the human condition.[27–29] Hence, in these experiments, this model was used to establish the relationship between in vivo measures of the GCILP thickness and cell density in the macula region of healthy and diseased eyes. In addition, we aimed to determine the relationship between visual thresholds, stimulus size, and RGC counts in the macula region using the nonhuman primate experimental glaucoma model.

Methods

Subjects

The subjects for these experiments were 13 rhesus monkeys (*Macaca mulatta*). Ten animals (5 OD, 5 OS) were used for establishing test-retest variability and normative data for 10-2 perimetry using Goldmann size I through V stimuli. Four of these 10 animals (OHT-71, OHT-72, OHT-73, OHT-74) had induced unilateral experimental glaucoma (all right eyes), and both eyes were followed longitudinally with 10-2 perimetry to varying stages of experimental glaucoma. Both eyes of one of the four animals (OHT-72) and three additional unilateral experimental glaucoma animals naive to 10-2 perimetry (OHT-64, OHT-66, OHT-67) were used for establishing the relationship between OCT-derived GCIPL thickness and histologic retinal ganglion cell density. All experimental and animal care procedures were reviewed and approved by the Institutional Animal Care and Use Committee of the University of Houston. The use of animals for these experiments adhered to the ARVO statement for the Use of Animals in Ophthalmic and Vision Research and to the National Institutes of Health guidelines for the care and use of laboratory animals.

Animal Sedation

Before conducting laser or scanning procedures, monkeys were anesthetized with an intramuscular injection of ketamine (20 mg/kg) and xylazine (0.8 mg/kg) and treated with a subcutaneous injection of atropine sulfate (0.04 mg/kg). While animals were sedated, body temperature was monitored and maintained using a thermal blanket (TC 1000 temperature controller; CWE, Ardmore, PA, USA); heart rate and pulse were monitored with a pulse oximeter (model 9847V; Nonin Medical, Inc., Plymouth, MN, USA). The animal's head was stabilized using mouth and occipital bars. For retinal imaging, 1% tropicamide was used to dilate the pupils, the eyelids were kept open with a lid speculum, and a plano rigid gas-permeable contact lens was used to maintain optical clarity and corneal hydration.

Laser-Induced Ocular Hypertension

Experimental glaucoma was induced by scarring the trabecular meshwork using a 532-nm diode laser (Visulas 532; Carl Zeiss Meditec, Jena, Germany). Contiguous laser burns (1.0 W, 0.5 seconds, 50-µm spot size) were applied to the trabecular meshwork through a laser gonioscopy lens (Ocular Kaufman; Ocular Instruments, Bellevue, WA, USA). The initial procedure involved 270° of the drainage angle, followed with re/treatment of 180° at 3-week intervals until sustained elevated intraocular pressures were achieved. Intraocular pressure was measured using the Tono-Pen XL (Reichert, Inc., Depew, NY, USA) at each OCT imaging session, which were nominally at 2-week intervals. For each animal, cumulative IOP was calculated as previously described.[30,31]

Optical Coherence Tomography

All OCT scans were acquired using the Spectralis HRA+OCT system (Heidelberg Engineering, Heidelberg, Germany) with high-resolution setting. The scan protocols included a (1) 97-line, 20° × 20° raster scan centered on the optic nerve head; (2) 12-line, 20° radial scan centered on the optic nerve head; and (3) 97-line, 20° × 20° scan centered on the macula. Scans were exported as raw (.vol) files and analyzed using custom software (MATLAB; The MathWorks, Inc., Natick, MA, USA).[32,33]

To determine the transverse extent of the retina imaged, at each scan session, ocular biometry was obtained using the Lenstar LS900 (Haag-Streit, Koeniz, Switzerland) and used to construct a three-surface schematic eye.[34] Subsequently, and as previously described, transverse retinal scaling (µm/deg) was calculated from the second nodal plane to the retina, assuming a spherical retinal surface.[33] No adjustments were made for axial scaling, which is not dependent on ocular magnification.

Optic nerve head (ONH) morphology and circumpapillary retinal nerve fiber layer (RNFL) thickness for each of the seven experimental glaucoma animals were analyzed as previously described.[32,33] In brief, radial b-scans were first scaled to a 1:1 aspect ratio using the computed transverse scaling. Borders of the inner limiting membrane and Bruch's membrane were manually corrected for segmentation errors, and on each b-scan, Bruch's membrane opening (BMO) was manually marked. Subsequently, the minimum distance from the BMO to the inner limiting membrane was used to calculate the mean minimum rim width (MRW). The BMO was transposed to the raster scan centered on the optic nerve head, after registering the two scanning laser ophthalmoscope images. An elliptical scan path 550 µm from the BMO was calculated and used to interpolate a b-scan from the raster volume. The RNFL thickness was then calculated as

Investigative Ophthalmology & Visual Science

Downloaded from iovs.arvojournals.org on 01/18/2023

the perpendicular distance between the inner limiting and nerve fiber layer/ganglion cell layer borders.

As with ONH scans, b-scans of the macula were processed using programs written in MATLAB. Instrument segmentation errors of the inner limiting membrane and Bruch's membrane were first corrected. Subsequently, the junctions between (1) the nerve fiber and ganglion cell layer and (2) the inner nuclear and inner plexiform layers were manually delineated. Any visible retinal vasculature that contacted the nerve fiber layer was included in that layer. The perpendicular distance between the nerve fiber/ganglion cell layer junction and inner nuclear/inner plexiform layer junction was used to compute the GCIPL. Using these methods, the interobserver (KA-B and NP) test-retest repeatability (2.77 × within-subject standard deviation (Sw)) for the average GCIPL thickness for any single b-scan was 2.9 µm, with a coefficient of variation (CV) of 1.94%. For structure-function and histologic correspondence, thickness maps for each raster scan were linearly interpolated for the 20° × 20° scanned region.

Tissue Preparation and Confocal Imaging

For the four animals used for histologic correspondence, a fluorescein angiogram was performed between 1 and 3 weeks prior to euthanasia. Subsequently, after collecting endpoint OCT images, animals were euthanized through an overdose (100 mg/kg) of sodium pentobarbital (Fatal-Plus; Vortech Pharmaceuticals, Dearborn, MI, USA). Following exsanguination with 0.1 M PBS, animals were perfusion fixed with 4% paraformaldehyde and the eyes enucleated. The retrobulbar optic nerve from experimental and control eyes was dissected approximately 2 mm posterior to the globe, cut to 0.5-mm sections, and placed in a solution of 2.5% glutaraldehyde and 2% paraformaldehyde. After the anterior segment was removed, the posterior eye cup was stored in 4% paraformaldehyde.

Following 24 hours in fixative, the retrobulbar optic nerve sections were postfixed in 2% osmium tetroxide, dehydrated, and embedded in EPON (EMBED - 812, Electron Microscope Sciences, Hatfield, PA) resin. Subsequently, 1-µm-thick sections were cut, mounted, and stained with p-phenylenediamine for light microscopy. The most complete and uniformly stained section from each sample was chosen, and the entire cross section of the nerve imaged using a ×100 objective (Olympus BX 53; Olympus, Tokyo, Japan). Subsequently, 100% of all myelinated axons from each nerve were manually counted on an image analysis platform (Bioquant Imaging System, NOVA; R&M Biometrics, Inc., Nashville, TN, USA) attached to the microscope system. We have previously assessed repeatability of these methods, using tissue from additional animals to those in the current study, comparing axon counts from two separate well-stained optic nerve sections from eight eyes (four eyes experimental glaucoma and four normal controls, 2.77 × Sw = 48,228 axons, CV = 3.19%). Furthermore, axon counts using this method have been compared to circumpapillary RNFL thickness for 15 eyes with experimental glaucoma (including the four animals used for histologic work in the current study) and 12 normal control eyes (Antwi-Boasiako K, et al. *IOVS* 2017;58(8):4025). Axon counts using the methods described are linearly related to the circumpapillary RNFL thickness (Fig. 1) and similar to that previously reported.[35]

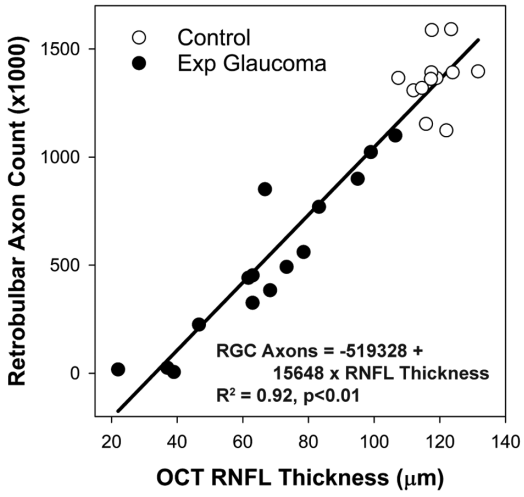

Figure 1. Relationship between endpoint circumpapillary RNFL thickness at 550 µm from Bruch's membrane opening and retrobulbar axon counts.

Using the last OCT macula scan as a guide, the central retina was dissected from the eyecup at least 0.25 mm from each side of the extent of the 20° × 20° raster scan border. After removal of sclera and choroid, macula tissues were washed in PBS and incubated with DRAQ5 (1, 5-bis [2-(dimethylamino) ethyl] amino-4, 8-dihydroxyanthracene-9, 10-Dione: a cell permeable fluorescent DNA dye; ThermoFisher Scientific, Rockford, IL, USA; 1:1000 in PBS) at 4°C for 48 hours, rinsed in PBS, and flat mounted in Vectashield (Vector Laboratories, Burlingame, CA, USA). For orientation, images of the tissue were first captured at 10× magnification using confocal microscopy (Leica SPC2; Leica Microsystems, Inc., Buffalo Grove, IL, USA). Overlapped regions were montaged, and vascular structures were used to register the mounted tissue to the previously captured fluorescein angiogram and GCIPL thickness map from the last scan session. From this registration, tissue shrinkage from processing (between 4% and 8%) was accounted for, and all subsequent physical dimensions were computed based on the in vivo scaling. For cell nuclei quantification, two diagonal strips, centered on the fovea, were imaged at 40× magnification with a minimum of 5% overlap. For each of the 40× regions (375 µm in length and width), a z-stack from the inner limiting membrane to the inner nuclear layer was acquired with 2 µm spacing (Fig. 1A).

OCT and Histologic Correspondence

All cell marking and comparisons to the underlying OCT GCIPL thickness were done using programs written in MATLAB. A 300-µm bounding box was overlaid on each confocal stack, and individual cells were marked ensuring that cells at varying depths were only counted once (each nucleus traversed between three and four z-sections). Elongated nuclei, which were typically associated with vasculature, were not marked. The bounding box was subdivided into nine 100-µm square regions, whose cell density was compared to the underlying registered OCT-derived GCIPL thickness (Fig. 1B). A 100-µm square region was selected as it included, at minimum, two OCT b-scans. To determine the repeatability of cell counts, nuclei were

Investigative Ophthalmology & Visual Science

Downloaded from iovs.arvojournals.org on 01/18/2023

recounted for two healthy and two experimental glaucoma eyes.

Behavioral Perimetry

Visual thresholds were quantified using static threshold perimetry with a clinical Humphrey Field Analyzer (HFA 750i; Carl Zeiss Meditec, Inc., Dublin, CA, USA), which was attached to a nonhuman primate testing chamber. Animals were acclimated to sit in a primate chair, which was positioned such that the tested eye was at the correct viewing distance and centered with respect to the perimeter's fixation light-emitting diode (LED). Each monkey was trained to press a response lever to initiate a trial and given up to 700 ms to respond to the presented visual stimulus. True positives were reinforced with orange drink, while false positives and misses were not punished, but no juice reinforcement was offered. To maintain fixation, the central LED of the perimeter was used as a dimming stimulus, which was controlled through an external program. Approximately 20% of all trials were central fixation, and the remaining trials were released to the native perimeter full-threshold algorithm, which was paused between trials. Additional details on perimetry in nonhuman primates have been previously reported.[36] Using this protocol, animals worked approximately 2 hours each day, completing a single 10-2 visual field at each session. Once animals had reliable responses (less than 5% false positives and false negatives), at least two 10-2 fields were obtained from one eye of 10 animals (five right eyes and five left eyes), using size I to V stimuli, which were used to determine normative means, standard deviations, and repeatability for each test location. In addition, spatial summation was assessed at four oblique locations (1.41, 4.24, 7.07, and 9.06) for perimetric thresholds converted from attenuation values (dB) to differential light intensities (DLSs) in candelas per meter squared (cd/m^2).

$$\textit{Differential Light Sensitivity (DLS)} = \frac{10^{\frac{(40-dB)}{10}}}{\pi}$$

Four of the animals performing perimetry were subsequently followed longitudinally with OCT and 10-2 perimetry, after induction of experimental glaucoma. These animals had the lowest mean sensitivity test-retest variability of <2 dB prior to experimental glaucoma and were able to complete a set of visual fields (size I–V) in 10 to 14 days. One animal was followed until the first detectable MRW change, one was followed until the first circumpapillary RNFL change, and two were monitored until moderate-stage neuropathy. On average, a complete set of perimetry data (size I–V) can be collected in 1 week. However, in most instances, animals would not provide reliable data at the start of the week and were sedated for imaging and did not perform perimetry at the end of every other week. Based on the working hypothesis, priority was on obtaining at least one size I to III field on a weekly basis. Hence, complete sets (sizes I–IV) were collected approximately every 10 to 14 days from experimental glaucoma eyes and every 4 to 6 weeks from control eyes.

Structure-Function Correspondence

To relate visual thresholds to GCIPL thickness, test locations were displaced using equations described by Drasdo[15,37] but scaled to the nonhuman primate eye. For each threshold test location, the GCIPL volume was calculated as the average thickness multiplied by the stimulus size, after accounting for individual differences in lateral scaling and subtracting residual thickness. The residual thickness was determined based on the relationship between GCIPL thickness and cell density (Fig. 2C and as described in the results). Akaike's information criterion (AIC) was used to determine if a single line, exponential decay, or segmental regression (spatial summation) resulted in the best fit.

Statistical Analysis

Descriptive statistics were used to describe the mean and standard deviations for visual thresholds and all structural measures. Repeatability of both structural and functional measures was assessed using the square root of the mean intrasubject variance[38] and the coefficient of variation. Stepwise regression was used to determine the relationship between GCIPL thickness and cell density. AIC was used to determine if a straight line, exponential decay, or segmental regression (spatial summation) resulted in the best fit for the relationship between (1) GCIPL volume and DLS and (2) RGC counts and DLS. For segmental fits of grouped data, the unconstrained slope of the first segment was compared to a slope of −1, as predicted by spatial summation. Statistical analysis was performed in either GraphPad (GraphPad Software, San Diego, CA, USA) or SPSS (IBM Corp., Armonk, NY, USA), and all plots were generated in SigmaPlot (Systat Software, Inc., San Jose, CA, USA).

Results

Relationship Between OCT GCIPL Thickness and Cell Density

The four animals used for histologic correspondence had stable OCT structure measures (less than repeatability change) for at least 4 weeks prior to the last imaging session. At their respective endpoints, the extent of experimental glaucoma based on percent retrobulbar axon content compared to the control eye was representative of early (OHT-67), mild (OHT-64), moderate (OHT-71), and severe (OHT-66) loss (Table 1).

The interobserver agreement of cell density from manual marking of confocal z-stacks was assessed for 108 regions measuring 100 × 100 µm of two healthy and two glaucoma eyes. Repeatability (2.77 × Sw) based on these markings was 822.7 cells/mm^2, CV = 3.01%. For the four normal control eyes, the peak cell density was 63,052 ± 9238 cells/mm^2, at an eccentricity of 3.3° (Fig. 3A). This corresponded with the peak GCIPL thickness from the same animals, which was 87.7 ± 2.2 µm at an eccentricity of 3.9°.

Following registration of the confocal z-stacks to endpoint in vivo imaging (Fig. 2), the cell densities and GCIPL thickness measures were compared for 1611 (715 control and 896 experimental glaucoma) similar 100 × 100-µm regions with stepwise multiple regression analysis. To determine the best fit, model predictors included GCIPL thickness, eccentricity, individual subjects, and disease state. While a significant linear relationship was found between GCIPL thickness and RGC density (Fig. 3B, slope = 819 cells/mm^2/µm, R^2 = 0.62, P < 0.01), a best fit was achieved when eccentricity was included (Fig. 3C, P < 0.01, R^2 = 0.74, lowest AIC). The relationship was not determined to be different between subjects, and although disease state was related to GCIPL thickness (P < 0.01), it was not iden-

Investigative Ophthalmology & Visual Science

Downloaded from iovs.arvojournals.org on 01/18/2023

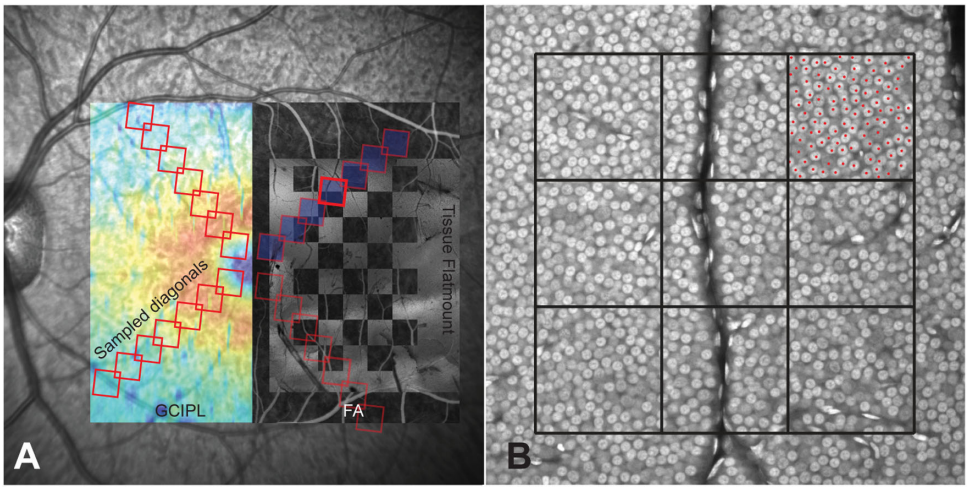

Figure 2. (**A**) The *right half* of the image illustrates the registration of the fluorescein angiogram and tissue flat mount, which was aligned to the GCIPL thickness map. The z-stacks at 40× magnification were acquired in four diagonals centered on the fovea. (**B**) Single image from a z-stack of the *highlighted* region in **A**. For each z-stack, all cells within a 300-µm bounding box were counted. The region was subdivided into nine 100 × 100 µm (marked cells illustrated for the *upper right sector* only), and cell densities within these regions compared to the corresponding average GCIPL thickness.

Table 1. Endpoint Subject Characteristics for Animals Used for Histological Correspondence to OCT Measures

Subject	Eye	Cumulative IOP (mm Hg·days)	Mean IOP (mm Hg)	RNFL Thickness (µm)	MRW (µm)	Retrobulbar Axon Counts
OHT-64	Experimental	6128	22.15	83	92	769,461 (55.3)
	Control		14.45	117	275	1,391,449
OHT-66	Experimental	9293	30.29	47	60	224,997 (16.5)
	Control		14.56	107	308	1,365,975
OHT-67	Experimental	9951	25.22	106	243	1,099,277 (78.7)
	Control		13.00	132	428	1,396,100
OHT-71	Experimental	13484	35.88	68	47	383,852 (33.3)
	Control		15.74	116	280	1,153,384

The number in parentheses indicates the percentage of control eye retrobulbar axon counts.

tified as a significant variable in the multiple regression analysis. The best-fit equation (cell density = −7281 + 815 × GCIPL thickness (µm) – 2497 × eccentricity (deg)) was subsequently used for all estimations of RGC counts from localized GCIPL thickness. In addition, solving this equation for a zero RGC count, the residual GCIPL thickness can be estimated as 8.93 + 3.06 × eccentricity (deg).

Spatial Summation and Normative 10-2, Sizes I to V

Ten animals were successfully trained to perform 10-2 perimetry, and at minimum, two visual fields with all five stimulus sizes, from each animal, were obtained with 0% false-positive and false-negative errors. Data from one eye of

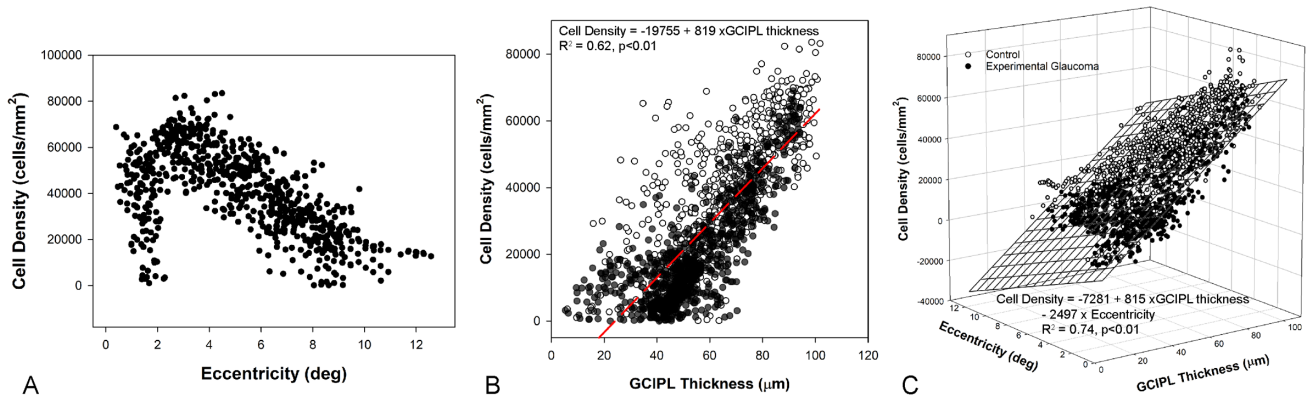

Figure 3. (**A**) Cell density in the retinal ganglion cell layer as a function of eccentricity measured from four control eyes. (**B**) The relationship between GCIPL thickness and cell density (**B**) improves when eccentricity is included (**C**).

Investigative Ophthalmology & Visual Science

Downloaded from iovs.arvojournals.org on 01/18/2023

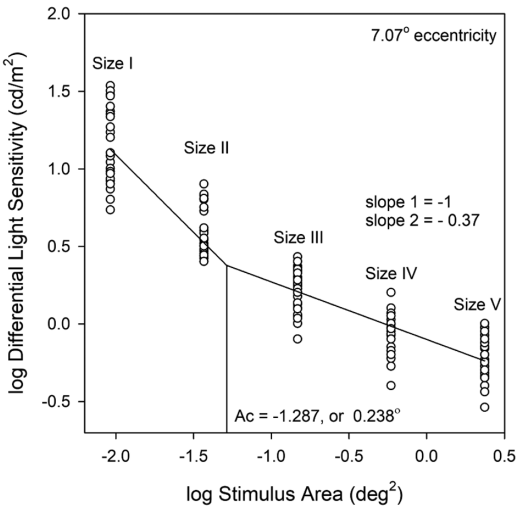

Figure 4. Plot of log differential light sensitivity versus log stimulus area for a representative eccentricity of 7.07° from healthy control eyes. The plot illustrates determination of the critical area (Ac) based on a segmental fit to the data.

each subject (five right and five left eyes) were used to establish normative values. As expected, the averaged mean sensitivity across the 10-2 sampled region was lower for smaller stimuli (size I, 25.1 ± 1.0 dB; size II, 29.3 ± 0.8 dB; size III, 32.9 ± 0.6 dB; size IV, 35.6 ± 0.6 dB; size V, 37.5 ± 0.5 dB; $P < 0.01$), and thresholds increased with eccentricity ($R^2 = 0.96$, $P < 0.01$). Similarly, the intersubject standard deviation of thresholds ($R^2 = 0.56$, $P < 0.01$) and intrasubject repeatability ($R^2 = 0.53$, $P < 0.01$) were dependent on both stimulus size and eccentricity, with smaller stimuli and more eccentric locations having higher variability. The mean threshold, standard deviations, and intrasubject variability for each test location and stimulus size are provided in the supplementary Excel spreadsheet.

Based on spatial summation (Ricco's law), the relationship between stimulus size and visual sensitivity was fit using a two-line segmental regression with least squares, where the slope of the first segment was constrained to −1.[26,39] The intersection of the two segments is the critical area (Ac, Fig. 4), which increased with eccentricity and was smaller than a size III stimulus across the 10-2 field (Table 2).

Visual Thresholds and Structural Correspondence in Experimental Glaucoma

Four of the 10 animals had right eye–induced experimental glaucoma and were monitored longitudinally (Table 3).

Table 2. Critical Area Diameter for Four Eccentricities in the 10-2 Visual Field

Eccentricity (Degrees)	Critical Area (Diameter in Degrees ± SE)
1.41	0.239 ± 0.031
4.24	0.249 ± 0.031
7.07	0.256 ± 0.030
9.06	0.259 ± 0.038

Two animals, OHT-71 and OHT-72, showed moderate loss of RNFL thickness, and both animals also had significant reduction of visual field sensitivity as determined with a size III stimulus; OHT-71 had a 5.02-dB reduction in mean sensitivity and OHT-72 a reduction of 2.81 dB. For OHT-73, data were collected until the first time point at which RNFL thickness had decreased below test-retest, and this animal had a reduction in sensitivity as determined with only size I (3.78 dB mean sensitivity) and size II stimulus (2.44 dB mean sensitivity). In contrast, OHT-74, who had a significant reduction in MRW but did not have a reduction in RNFL thickness exceeding repeatability, had no loss of sensitivity with any stimulus size (<1.2-dB loss of mean sensitivity).

The relationship between GCIPL volume and DLS was compared using nonlinear regression. For this analysis, perimetry data (sizes I–V) from the last four time points (approximately 1.5 months of data and with relatively stable structure and functional measures) for all glaucoma eyes and the last time point for the control eyes were used. In all instances, GCIPL structural measures were obtained within ±7 days of the functional data. Of the three models (linear, exponential decay, and segmental), a segmental fit achieved the lowest AIC for the grouped and eccentricity separated data. Furthermore, the slope of the first segment was not significantly different from −1 ($P = 0.81$), following that predicted by spatial summation. Subsequently, all GCIPL volume versus DLS data were fit with a segmental function with the slope of the first segment constrained to −1. Furthermore, when separated to the nine eccentricities of the 10-2, the segment intercepts and second line slopes were similar ($P = 0.26$, Table 4, Fig. 5A), and subsequently, all GCIPL volume data were plotted on a single plot, without including eccentricity. For this combined data set (all four animals), the intersection of the two slopes for the control eyes was determined to be at a GCIPL volume of 2.58×10^5 µm³ (Fig. 5B), and smaller than that of the glaucomatous eyes, 2.65×10^5 µm³ ($P < 0.01$, Figs. 5C, 5D). This difference represents approximately 1 µm of GCIPL thickness for a size III stimulus, or a 1-µm difference in stimulus diameter for an average GCIPL thickness of 60 µm, which may not be clinically significant. Subsequently, GCIPL data

Table 3. Endpoint Subject Characteristics for Animals Used for Longitudinal Functional Assessment

Subject	Eye	Cumulative IOP (mm Hg· Days)	Mean IOP (mm Hg)	RNFL Thickness (µm)	MRW (µm)
OHT-71	Experimental	13,484	35.88	68	47
	Control		15.74	116	280
OHT-72	Experimental	18,478	34.47	78	141
	Control		15.03	117	367
OHT-73	Experimental	2038	24.94	110	204
	Control		14.44	116	332
OHT-74	Experimental	1654	23.86	109	193
	Control		13.43	112	307

Investigative Ophthalmology & Visual Science

Downloaded from iovs.arvojournals.org on 01/18/2023

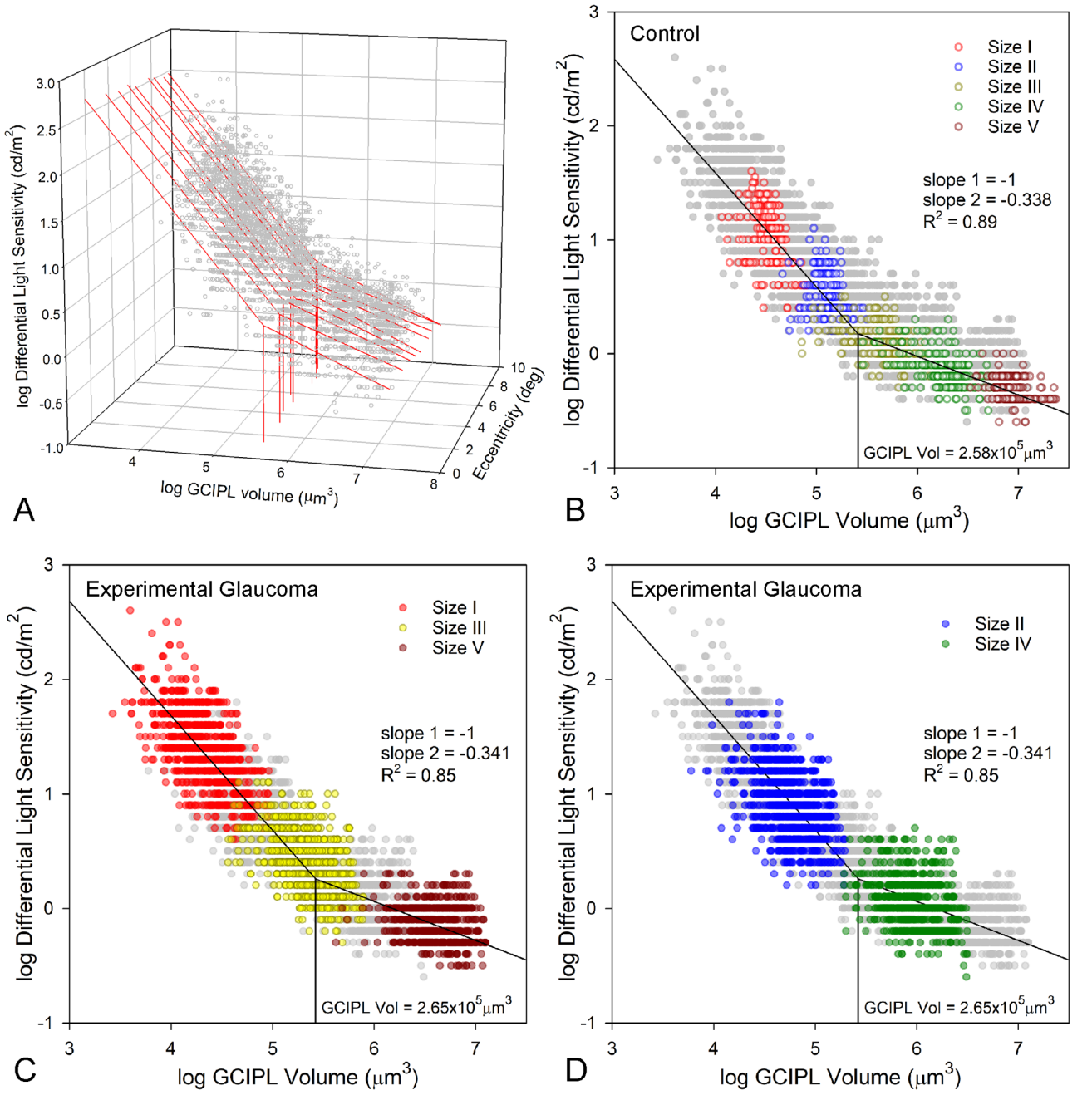

Figure 5. Relationship between log GCIPL volume, eccentricity, and log differential light sensitivity from four animals with experimental glaucoma (**A**). The *red plots* are segmental fits for each eccentricity. (**B**) Relationship between log differential light sensitivity and log GCIPL volume of combined eccentricities. The *colored symbols* represent different stimulus sizes from control eyes. To illustrate the distribution of data from experimental glaucoma, sizes I, III, and V are shown in **C** and sizes II and IV in **D**. The *gray symbols* in each plot represent data from eyes with experimental glaucoma.

were also transformed based on the histologic correspondence (Fig. 3C) to determine the relationship between visual thresholds and number of RGCs (Fig. 6). The segmental fit from this analysis suggests a steeper slope when fewer than 155.6 ± 6.5 RGCs are stimulated.

We subsequently used the segmental fit in Figures 5B–D to generate a model for predicting visual sensitivity from GCIPL thickness (Fig. 7). Because GCIPL volume is not a common clinical measure, thickness for this model was estimated for each stimulus size using the lateral magnification of an emmetropic NHP eye. The longitudinal data from the two animals monitored to more severe stages of neuropathy follow that of the predicted structure-function model (Figs. 7B, 7C).

The data plotted in Figure 5 show that while the majority of control eye size III stimuli fall on the shallow slope of the segmental fit, with experimental glaucoma, these data shift toward the steeper portion of the function. If Ac is dependent on the number of underlying RGCs, the data in Figure 5 would suggest a change in the critical area with

Investigative Ophthalmology & Visual Science

Downloaded from iovs.arvojournals.org on 01/18/2023

Table 4. Intersection and Second Line Slopes for Segmental Fits to Log Ganglion Cell Inner Plexiform Layer Volume and Log Differential Light Sensitivity for All 10-2 Eccentricities

Eccentricity	Intersection (Log GCIPL Volume)	Intersection – GCIPL Volume ($\times 10^5$ µm^3)	Second Slope	R^2
1.41	5.49	3.148	−0.367	0.81
3.16	5.50	3.170	−0.323	0.84
4.24	5.42	2.606	−0.342	0.85
5.10	5.46	2.851	−0.362	0.87
5.83	5.33	2.138	−0.389	0.88
7.07	5.50	3.170	−0.322	0.88
7.62	5.51	3.206	−0.283	0.87
8.60	5.41	2.547	−0.299	0.85
9.06	5.33	2.128	−0.373	0.83

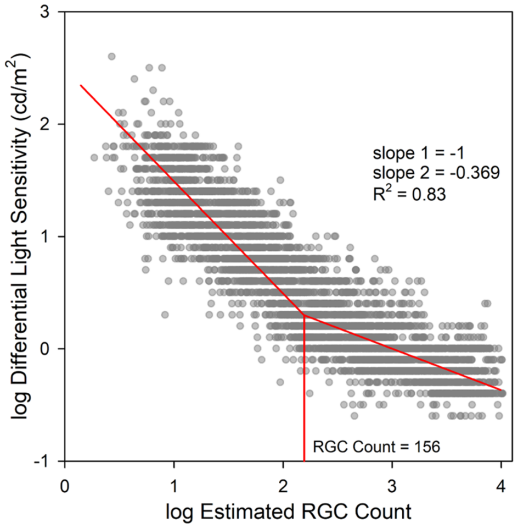

Figure 6. Relationship between number of RGCs in the stimulus area and visual sensitivity.

disease progression. In fact, all three animals with functional loss showed an increase in Ac ($P < 0.01$). Figure 8 illustrates these data for the animal with the greatest (OHT-71) and least (OHT-73) reduction in visual sensitivity. For the more severe subject, Ac was greater than that of a size III stimulus for the majority of eccentricities, while in the less severe subject, although a reduction in sensitivity was noted for size I and II stimuli, Ac was still smaller than that of a size III stimulus.

Discussion

Clinically, visual function in glaucoma is monitored using static, threshold perimetry with test protocols up to 30° from fixation, using stimuli spaced at 6° intervals, with central 10-2 and macula visual fields protocols with 2° stimulus spacing, usually reserved for patients with advanced glaucoma. However, with the introduction of high-resolution macula scans and quantification of inner retinal thickness, there has been a paradigm shift, as OCT studies show significant loss of macula inner retinal thickness at early stages of glaucoma.[5,10,40–42] Concurrently, there have been corresponding reports of detectable central 10-2 perimetric defects in early disease.[4,43,44] To better understand the structure-function relationships of the central visual field, we investigated the relationship between GCIPL thickness and histologic cell density, as well as the basic correspondence between GCIPL thickness and visual function. Overall, the data show that the quantitative relationship between perimetric thresholds and in vivo structure is dependent on a critical number of RGCs in the area underlying the visual stimulus.

In vivo GCIPL thickness is often used as a surrogate for RGC content but without histologic validation. A principal finding of the present study is the eccentricity-dependent relationship between GCIPL thickness and cell density. Specifically, for the same GCIPL thickness, locations closer to the foveola represent a greater cell density compared to more eccentric ones, and more eccentric locations have greater residual thickness. Although the histologic correspondence was limited to the central 10°, the results suggest that outside of this region, the GCIPL thickness would have limited value in estimations of cell density where the ganglion cell layer is a monolayer. Due to the similarity with human eyes, although the investigation was conducted on macaque eyes, it is expected that this histologic relationship will translate to humans after accounting for size and scaling differences between the two species. In fact, a similar eccentricity-dependent correspondence can be implied in human eyes based on normal OCT-derived ganglion cell layer thickness and reported histologic RGC density.[45]

Most cells in the ganglion cell layer are RGCs, but the layer also has astroglia, and in healthy eyes, between 3% and 5% of cell bodies are displaced amacrine cells (peak cell density of 1200 cells/mm^2).[21,46] Similarly, a small percentage of RGCs is displaced.[47] A limitation of the current study is that all cell nuclei, other than those belonging to retinal vasculature, in the ganglion cell layer were included. Many attempts to label just RGCs using an antibody against RNA-binding protein with multiple splicing (RBPMS)[48] were made, but antibody penetration was limited to ~30 µm and not sufficient to label all RGCs for a flat mount, regardless of fixation or antigen retrieval techniques. While RGC estimations using RBPMS could be made with cross-sectional samples, the flat-mount technique used was not only more accurate but also essential for registration with OCT thickness maps. Furthermore, cross sections through the macula region in control and experimental glaucoma eyes suggest a similar number of non-RBPMS labeling cells and similar densities to those previously reported (Fig. 9), which would need to be accounted for when determining the critical number of RGCs. These methodologic differences could account for the greater peak cell density of 63,052 ± 9238 cells/mm^2, compared to previous studies of primate eyes: Wassle et al.[49] (48,000 cells/mm^2), Rolls and Cowey[50] (50,000 cells/mm^2), and Silveira et al.[51] (49,000 cells/mm^2).[21]

For clinical translation, cell density in the nonhuman primate is almost double that reported for human eyes of 35,100 cells/mm^2.[19] Although a portion of this discrepancy could be explained by methodology, it is likely a reflection of differences in eye size. Specifically, both human and nonhuman primate eyes have approximately the same number of RGCs, have similar visual function, but have significantly different eye size and therefore total retinal surface area.[36,52] Assuming the underlying visual pathways are similar in these two species, the neural density per visual angle should also coincide. Based on an average retinal scaling for a rhesus macaque of 218 µm/deg (18.67 mm axial length)[53] and 291 µm/deg (24.09 mm axial length)[34] for a human, a 1° squared region in the area of peak density would

Investigative Ophthalmology & Visual Science

Downloaded from iovs.arvojournals.org on 01/18/2023

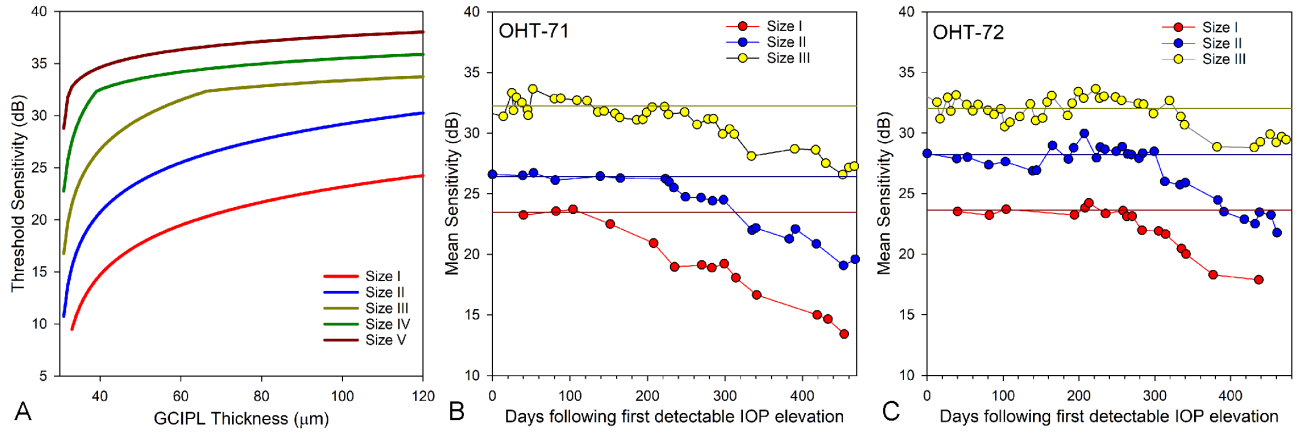

Figure 7. (**A**) Model of DLS as a function of stimulus size and GCIPL for the central 10-2 field regions. (**B**, **C**) Longitudinal mean sensitivity data (averaged thresholds across the central 10-2 region) for the two subjects with moderate experimental glaucoma. Time points are referenced to the first detectable change in IOP.

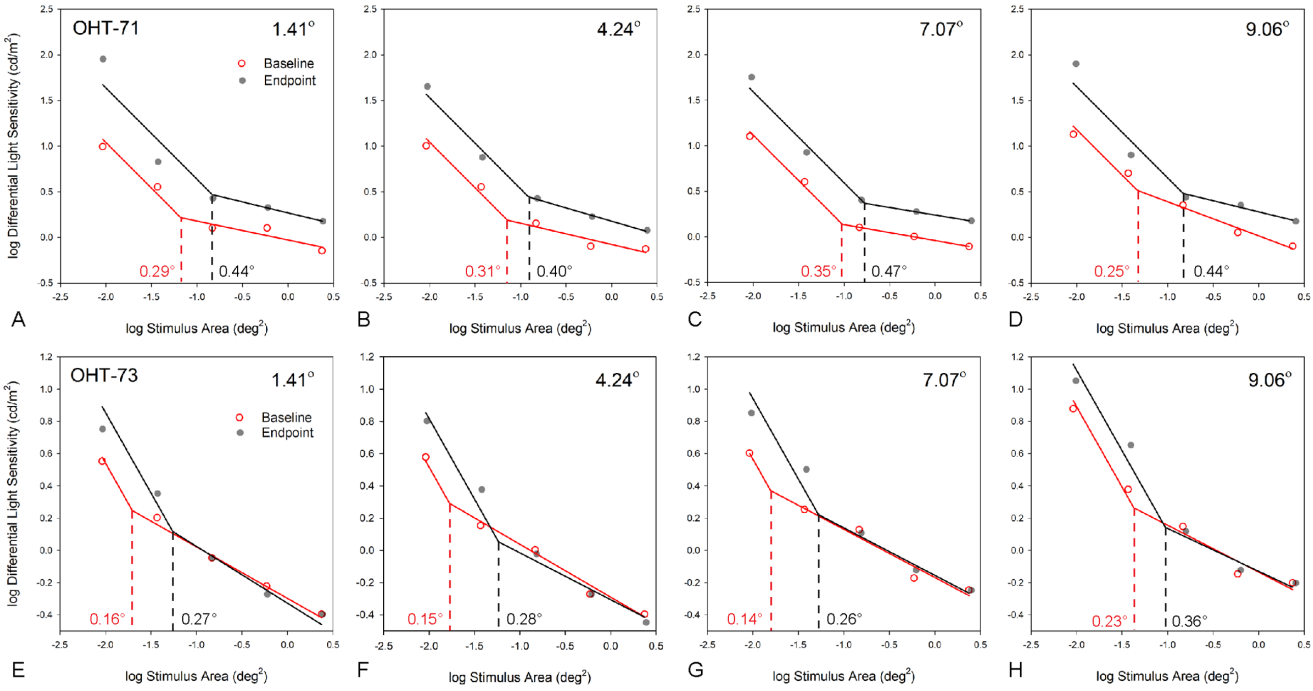

Figure 8. Spatial summation functions comparing baseline to endpoint for two animals, OHT-71 (**A–D**) and OHT-73 (**E–H**). With RGC loss, both subjects have an increase in the critical area.

include 2996 and 2972 RGCs in the rhesus and human retinas, respectively. These structural similarities are critical for investigations of structure-function correspondence and translation to the human condition.

The macula region is essential for high acuity; hence, detection and quantification of functional changes in this region are of critical importance. In principle, functional measures should coincide with structural measures of RGCs. However, the relationship between inner retinal thickness and visual thresholds using standard clinical techniques has been modest in nature, with significant structural losses seen prior to a decrease in visual sensitivity.[16–18] For example, at the area of peak cell density, an approximately 40-μm GCIPL thickness loss is needed prior to a 5-dB loss of visual threshold at that location,[16] corresponding to our observations and model (Fig. 7A) in the nonhuman primate. Similarly, the nonlinear model, developed in the nonhuman primate, has a shallower slope in the macula compared to more peripheral regions, suggesting smaller decreases in visual function compared to structure in this region.[54] Hence, using standard functional testing, when there is mild thinning of central inner retinal thickness, visual function in the 10-2 region may be statistically normal. Therefore, it is not surprising that while some studies have clearly shown the potential of 10-2 perimetry for early detection of perimetric defects,[43,44,55] others would suggest that detection of disease is similar using traditional 24-2 and macula visual fields.[56,57]

Investigative Ophthalmology & Visual Science

Downloaded from iovs.arvojournals.org on 01/18/2023

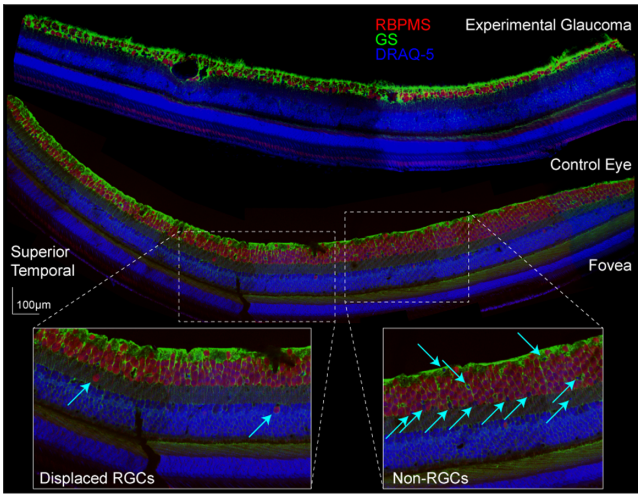

Figure 9. Sections from similar regions of a control and fellow experimental glaucoma eye, labeled with DRAQ-5, RBPMS, and glutamine synthetase (GS). In the control eye, there are a total of 946 RBPMS-labeled cells, 5 displaced to the inner plexiform layer or inner nuclear layer, and 17 are in the nerve fiber layer. In the ganglion cell layer, there are a total of 26 nuclei whose cytoplasm does not label for RBPMS, representing approximately 2.7% of the cells in the layer. There are no displaced RGCs in the experimental glaucoma eye, but 39 of the 231 cell nuclei do not label for RBPMS. The *cyan arrows* indicate displaced RGCs and cells not labeled with RBPMS.

A likely explanation for the relatively poor structure-function relationship within the central 10° could be the use of a nonoptimal stimulus size. Under photopic conditions, the critical area, also referred to as Ricco's area, is less than 10.1 min or 0.16° at a 10° eccentricity, and for stimuli smaller than this area, there is a reciprocal relationship between stimulus area and thresholds (slope = −1).[25,39] For stimuli larger than the critical area, a relationship between stimulus size and threshold still exists, but with a much shallow slope following Piper's law, or probability summation. While the area of spatial summation does vary with background illumination,[39,58] the Goldmann size III stimulus (0.43) exceeds this area for all locations of the 10-2 field when performed on a 10-cd/m^2 background, both humans[24] and nonhuman primates (Table 2).

In the present study, the relationship between GCIPL volume and visual thresholds was best fit using a segmental function with similar characteristics to spatial summation. While the precise physiology of spatial summation remains unknown, it is thought to be related to the underlying RGC properties along with cortical pooling.[59–61] With respect to RGC critical numbers, our data suggest that the critical area under the conditions of clinical perimetry represents approximately 156 RGCs. In principle, this is similar to the number of midget cells predicted to represent the critical area in human subjects.[62] In addition, with disease progression, the nonhuman primate data suggest that there is an increase in the critical area, which is similar to findings in human subjects.[63]

With glaucomatous disease, there was no change in the GCIPL volume to sensitivity relationship, but larger-sized stimuli were also on the steeper portion of the threshold-versus-area function. In particular, visual sensitivities of healthy eyes for size III stimuli fall on the shallower slope of the threshold-versus-area function, but as glaucoma disease progresses, the sensitivities fall on the steeper sloped portion of the function (Fig. 6B versus Fig. 6C), which complicates how macular function is assessed during disease progression. Specifically, the rate of change of visual thresholds would be slower prior to the stimulus reaching the critical number of RGCs, after which the rate is predicted to significantly increase. Furthermore, these findings would suggest that standard metrics from 10-2 perimetry are not suitable for assessing quality of vision. This is supported by the relatively weak correspondence between standard visual field metrics and vision-related quality of life.[64,65]

It is possible to improve quantification of visual function as there is strong correspondence between structure and function using smaller stimuli. Even at early stages of neuropathy, a reduction of visual thresholds can be quantified when the stimulus is smaller than the critical area. However, there are limitations to reducing stimulus area, because smaller stimuli, especially size I, have larger inter- and intraindividual variability, which would be reflected in the statistics of disease detection using perimetric global indices. Similarly, although size II stimuli had comparable repeatability to that of size III, the stimulus size has a limited dynamic range. Hence, the use of smaller stimuli is not clinically practical for all patients and stages of neuropathy. Ideally, testing of visual function would be directed by in vivo inner retinal thickness measures, where test stimuli can be selected based on localized disease severity and obtained threshold measures scaled to maintain linearity for progression analysis.[23,66,67] We believe that the histologic correspondence and structure-function model will aid in the development of such tools.

In conclusion, the GCIPL thickness is linearly related to cell density but is dependent on eccentricity. For all locations tested by 10-2 perimetry, the standard size III stimulus exceeds the critical area for spatial summation, and in early disease, loss of visual thresholds is greater with smaller stimuli. Regardless of stimulus size, visual thresholds are dependent on the corresponding number of RGCs stimulated.

Acknowledgments

Supported by National Institutes of Health (R01 EY029229, NIH P30 EY007551) and the University of Houston Mary Murphy Research Endowment.

Disclosure: **K. Antwi-Boasiako,** None; **L. Carter-Dawson,** None; **R. Harwerth,** None; **M. Gondo,** None; **N. Patel,** None

References

1. Anctil JL, Anderson DR. Early foveal involvement and generalized depression of the visual field in glaucoma. *Arch Ophthalmol*. 1984;102:363–370.
2. King D, Drance SM, Douglas GR, Wijsman K. The detection of paracentral scotomas with varying grids in computed perimetry. *Arch Ophthalmol*. 1986;104:524–525.
3. Stamper RL. The effect of glaucoma on central visual function. *Trans Am Ophthalmol Soc*. 1984;82:792–826.
4. Hood DC, Raza AS, de Moraes CGV, et al. Initial arcuate defects within the central 10 degrees in glaucoma. *Invest Ophthalmol Vis Sci*. 2011;52:940–946.
5. Tan O, Chopra V, Lu AT, et al. Detection of macular ganglion cell loss in glaucoma by Fourier-domain optical coherence tomography. *Ophthalmology*. 2009;116:2305–2314, e2301–e2302.

Downloaded from iovs.arvojournals.org on 01/18/2023

6. Giovannini A, Amato G, Mariotti C. The macular thickness and volume in glaucoma: an analysis in normal and glaucomatous eyes using OCT. *Acta Ophthalmol Scand Suppl*. 2002;236:34–36.
7. Lederer DE, Schuman JS, Hertzmark E, et al. Analysis of macular volume in normal and glaucomatous eyes using optical coherence tomography. *Am J Ophthalmol*. 2003;135:838–843.
8. Zeimer R, Asrani S, Zou S, Quigley H, Jampel H. Quantitative detection of glaucomatous damage at the posterior pole by retinal thickness mapping: a pilot study. *Ophthalmology*. 1998;105:224–231.
9. Mwanza JC, Budenz DL, Godfrey DG, et al. Diagnostic performance of optical coherence tomography ganglion cell–inner plexiform layer thickness measurements in early glaucoma. *Ophthalmology*. 2014;121:849–854.
10. Nouri-Mahdavi K, Nowroozizadeh S, Nassiri N, et al. Macular ganglion cell/inner plexiform layer measurements by spectral domain optical coherence tomography for detection of early glaucoma and comparison to retinal nerve fiber layer measurements. *Am J Ophthalmol*. 2013;156:1297–1307.e1292.
11. Hood DC. Improving our understanding, and detection, of glaucomatous damage: an approach based upon optical coherence tomography (OCT). *Prog Retin Eye Res*. 2017;57:46–75.
12. Mwanza JC, Oakley JD, Budenz DL, Chang RT, Knight OJ, Feuer WJ. Macular ganglion cell–inner plexiform layer: automated detection and thickness reproducibility with spectral domain-optical coherence tomography in glaucoma. *Invest Ophthalmol Vis Sci*. 2011;52:8323–8329.
13. Kim KE, Yoo BW, Jeoung JW, Park KH. Long-term reproducibility of macular ganglion cell analysis in clinically stable glaucoma patients. *Invest Ophthalmol Vis Sci*. 2015;56:4857–4864.
14. Garas A, Vargha P, Holló G. Reproducibility of retinal nerve fiber layer and macular thickness measurement with the RTVue-100 optical coherence tomograph. *Ophthalmology*. 2010;117:738–746.
15. Drasdo N, Millican CL, Katholi CR, Curcio CA. The length of Henle fibers in the human retina and a model of ganglion receptive field density in the visual field. *Vision Res*. 2007;47:2901–2911.
16. Raza AS, Cho J, de Moraes CG, et al. Retinal ganglion cell layer thickness and local visual field sensitivity in glaucoma. *Arch Ophthalmol*. 2011;129:1529–1536.
17. Sato S, Hirooka K, Baba T, Tenkumo K, Nitta E, Shiraga F. Correlation between the ganglion cell-inner plexiform layer thickness measured with cirrus HD-OCT and macular visual field sensitivity measured with microperimetry. *Invest Ophthalmol Vis Sci*. 2013;54:3046–3051.
18. Ohkubo S, Higashide T, Udagawa S, et al. Focal relationship between structure and function within the central 10 degrees in glaucoma. *Invest Ophthalmol Vis Sci*. 2014;55:5269–5277.
19. Curcio CA, Allen KA. Topography of ganglion cells in human retina. *J Comp Neurol*. 1990;300:5–25.
20. Hebel R, Holländer H. Size and distribution of ganglion cells in the human retina. *Anat Embryol*. 1983;168:125–136.
21. Muniz JAPC, de Athaide LM, Gomes BD, Finlay BL, Silveira LCdL. Ganglion cell and displaced amacrine cell density distribution in the retina of the howler monkey (*Alouatta caraya*). *PLoS ONE*. 2015;9:e115291.
22. Perry VH, Cowey A. The ganglion cell and cone distributions in the monkey's retina: implications for central magnification factors. *Vision Res*. 1985;25:1795–1810.
23. Khuu SK, Kalloniatis M. Standard automated perimetry: determining spatial summation and its effect on contrast sensitivity across the visual field. *Invest Ophthalmol Vis Sci*. 2015;56:3565–3576.
24. Khuu SK, Kalloniatis M. Spatial summation across the central visual field: implications for visual field testing. *J Vis*. 2015;15(1):6.
25. Anderson RS. The psychophysics of glaucoma: improving the structure/function relationship. *Prog Retin Eye Res*. 2006;25:79–97.
26. Riccò A. Relazione fra il minimo angolo visuale e l'intensità luminosa. Memorie della Societa Degli Spettroscopisti Italiani. 1877;6:B29–B58
27. Harwerth RS, Carter-Dawson L, Smith EL, 3rd Barnes G, Holt WF, Crawford ML. Neural losses correlated with visual losses in clinical perimetry. *Invest Ophthalmol Vis Sci*. 2004;45:3152–3160.
28. Harwerth RS, Quigley HA. Visual field defects and retinal ganglion cell losses in patients with glaucoma. *Arch Ophthalmol*. 2006;124:853–859.
29. Medeiros FA, Zangwill LM, Anderson DR, et al. Estimating the rate of retinal ganglion cell loss in glaucoma. *Am J Ophthalmol*. 2012;154:814–824.e811.
30. Harwerth RS, Smith EL, 3rd DeSantis L. Experimental glaucoma: perimetric field defects and intraocular pressure. *J Glaucoma*. 1997;6:390–401.
31. Yang H, Thompson H, Roberts MD, Sigal IA, Downs JC, Burgoyne CF. Deformation of the early glaucomatous monkey optic nerve head connective tissue after acute IOP elevation in 3-D histomorphometric reconstructions. *Invest Ophthalmol Vis Sci*. 2011;52:345–363.
32. Patel NB, Sullivan-Mee M, Harwerth RS. The relationship between retinal nerve fiber layer thickness and optic nerve head neuroretinal rim tissue in glaucoma. *Invest Ophthalmol Vis Sci*. 2014;55:6802–6816.
33. Patel NB, Luo X, Wheat JL, Harwerth RS. Retinal nerve fiber layer assessment: area versus thickness measurements from elliptical scans centered on the optic nerve. *Invest Ophthalmol Vis Sci*. 2011;52:2477–2489.
34. Rabbetts RB, Mallen EA. The schematic eye. In: Bennett AG, Rabbetts RB, eds. *Clinical Visual Optics*. London, UK: Butterworths; 1989:249–274.
35. Fortune B, Hardin C, Reynaud J, et al. Comparing optic nerve head rim width, rim area, and peripapillary retinal nerve fiber layer thickness to axon count in experimental glaucoma. *Invest Ophthalmol Vis Sci*. 2016;57:Oct404–Oct412.
36. Harwerth RS, Smith EL, III, DeSantis L. Behavioral perimetry in monkeys. *Invest Ophthalmol Vis Sci*. 1993;34:31–40.
37. Luo X, Patel NB, Rajagopalan LP, Harwerth RS, Frishman LJ. Relation between macular retinal ganglion cell/inner plexiform layer thickness and multifocal electroretinogram measures in experimental glaucoma. *Invest Ophthalmol Vis Sci*. 2014;55:4512–4524.
38. Bland JM, Altman DG. Measurement error. *BMJ*. 1996;313:744.
39. Wilson ME. Invariant features of spatial summation with changing locus in the visual field. *J Physiol*. 1970;207:611–622.
40. Tan O, Li G, Lu AT, Varma R, Huang D; Advanced Imaging for Glaucoma Study Group. Mapping of macular substructures with optical coherence tomography for glaucoma diagnosis. *Ophthalmology*. 2008;115:949–956.
41. Mwanza JC, Durbin MK, Budenz DL, et al. Glaucoma diagnostic accuracy of ganglion cell–inner plexiform layer thickness: comparison with nerve fiber layer and optic nerve head. *Ophthalmology*. 2012;119:1151–1158.
42. Moreno PA, Konno B, Lima VC, et al. Spectral-domain optical coherence tomography for early glaucoma assessment: analysis of macular ganglion cell complex versus peripapillary retinal nerve fiber layer. *Can J Ophthalmol*. 2011;46:543–547.

Investigative Ophthalmology & Visual Science

Downloaded from iovs.arvojournals.org on 01/18/2023

43. De Moraes CG, Hood DC, Thenappan A, et al. 24-2 Visual fields miss central defects shown on 10-2 tests in glaucoma suspects, ocular hypertensives, and early glaucoma. *Ophthalmology*. 2017;124:1449–1456.
44. Traynis I, De Moraes CG, Raza AS, Liebmann JM, Ritch R, Hood DC. Prevalence and nature of early glaucomatous defects in the central 10° of the visual field. *JAMA Ophthalmol*. 2014;132:291–297.
45. Raza AS, Hood DC. Evaluation of the structure-function relationship in glaucoma using a novel method for estimating the number of retinal ganglion cells in the human retina. *Invest Ophthalmol Vis Sci*. 2015;56:5548–5556.
46. Koontz MA, Hendrickson AE, Ryan MK. GABA-immunoreactive synaptic plexus in the nerve fiber layer of primate retina. *Vis Neurosci*. 1989;2:19–25.
47. Bunt AH, Minckler DS. Displaced ganglion cells in the retina of the monkey. *Invest Ophthalmol Vis Sci*. 1977;16:95–98.
48. Rodriguez AR, de Sevilla Muller LP, Brecha NC. The RNA binding protein RBPMS is a selective marker of ganglion cells in the mammalian retina. *J Comp Neurol*. 2014;522:1411–1443.
49. Wassle H, Grunert U, Rohrenbeck J, Boycott BB. Retinal ganglion cell density and cortical magnification factor in the primate. *Vision Res*. 1990;30:1897–1911.
50. Rolls ET, Cowey A. Topography of the retina and striate cortex and its relationship to visual acuity in rhesus monkeys and squirrel monkeys. *Exp Brain Res*. 1970;10:298–310.
51. Silveira LC, Picanco-Diniz CW, Sampaio LF, Oswaldo-Cruz E. Retinal ganglion cell distribution in the cebus monkey: a comparison with the cortical magnification factors. *Vision Res*. 1989;29:1471–1483.
52. Augusteyn RC, Maceo Heilman B, Ho A, Parel JM. Nonhuman primate ocular biometry. *Invest Ophthalmol Vis Sci*. 2016;57:105–114.
53. Qiao-Grider Y, Hung LF, Kee CS, Ramamirtham R, Smith EL III. Normal ocular development in young rhesus monkeys (*Macaca mulatta*). *Vision Res*. 2007;47:1424–1444.
54. Harwerth RS, Wheat JL, Fredette MJ, Anderson DR. Linking structure and function in glaucoma. *Prog Retin Eye Res*. 2010;29:249–271.
55. Grillo LM, Wang DL, Ramachandran R, et al. The 24-2 visual field test misses central macular damage confirmed by the 10-2 visual field test and optical coherence tomography. *Transl Vis Sci Technol*. 2016;5:15.
56. Sullivan-Mee M, Karin Tran MT, Pensyl D, Tsan G, Katiyar S. Prevalence, features, and severity of glaucomatous visual field loss measured with the 10-2 achromatic threshold visual field test. *Am J Ophthalmol*. 2016;168:40–51.
57. Wu Z, Medeiros FA, Weinreb RN, Zangwill LM. Performance of the 10-2 and 24-2 visual field tests for detecting central visual field abnormalities in glaucoma. *Am J Ophthalmol*. 2018;196:10–17.
58. Barlow HB. Temporal and spatial summation in human vision at different background intensities. *J Physiol*. 1958;141:337–350.
59. Pan F, Swanson WH. A cortical pooling model of spatial summation for perimetric stimuli. *J Vis*. 2006;6:1159–1171.
60. Glezer VD. The receptive fields of the retina. *Vis Res*. 1965;5:497–525.
61. Davila KD, Geisler WS. The relative contributions of pre-neural and neural factors to areal summation in the fovea. *Vis Res*. 1991;31:1369–1380.
62. Volbrecht VJ, Shrago EE, Schefrin BE, Werner JS. Spatial summation in human cone mechanisms from 0 degrees to 20 degrees in the superior retina. *J Opt Soc Am A Opt Image Sci Vis*. 2000;17:641–650.
63. Redmond T, Garway-Heath DF, Zlatkova MB, Anderson RS. Sensitivity loss in early glaucoma can be mapped to an enlargement of the area of complete spatial summation. *Invest Ophthalmol Vis Sci*. 2010;51:6540–6548.
64. Blumberg DM, De Moraes CG, Prager AJ, et al. Association between undetected 10-2 visual field damage and vision-related quality of life in patients with glaucoma. *JAMA Ophthalmol*. 2017;135:742–747.
65. Yamazaki Y, Sugisaki K, Araie M, et al. Relationship between vision-related quality of life and central 10° of the binocular integrated visual field in advanced glaucoma. *Sci Rep*. 2019;9:14990.
66. Rountree L, Mulholland PJ, Anderson RS, Garway-Heath DF, Morgan JE, Redmond T. Optimising the glaucoma signal/noise ratio by mapping changes in spatial summation with area-modulated perimetric stimuli. *Sci Rep*. 2018;8:2172.
67. Alluwimi MS, Swanson WH, Malinovsky VE, King BJ. Customizing perimetric locations based on en face images of retinal nerve fiber bundles with glaucomatous damage. *Transl Vis Sci Technol*. 2018;7:5.

Investigative Ophthalmology & Visual Science

Downloaded from iovs.arvojournals.org on 01/18/2023